

**GT2011-4\* \$- \$**

## **ANALYSIS OF A MICRO GAS TURBINE FED BY NATURAL GAS AND SYNTHESIS GAS: TEST BENCH AND COMBUSTOR CFD ANALYSIS**

**M. Cadorin, M. Pinelli, A. Vaccari**  
Dipartimento di Ingegneria (ENDIF)  
Università di Ferrara  
Ferrara, Italy

**R. Calabria, F. Chiariello, P. Massoli**  
Istituto Motori – CNR  
Napoli, Italy

**E. Bianchi**  
Turbec S.p.A.  
Corporeno di Cento, Italy

### **ABSTRACT**

In recent years, the interest in the research on energy production systems fed by biofuels is increased. Gaseous fuels obtained through biomass conversion processes such as gasification, pyrolysis and pyrogasification are generally defined as synthesis gas. The use of synthesis gas in small-size energy systems, such as those used for distributed micro-cogeneration, has not yet reached a level of technological maturity that could allow a large market diffusion. For this reason, further analyses (both experimental and numerical) have to be carried out to allow these technologies to achieve performance and reliability typical of established technologies based on traditional fuels.

In this paper, an experimental and numerical analysis of a combustor of a 100-kW Micro Gas Turbine fed by synthesis gas is presented. The work has been developed in the framework of a collaboration among the Department of Engineering of the University of Ferrara, the Istituto Motori CNR of Naples, and Turbec SpA of Cento (FE).

The main features of the microturbine MGT Turbec T100, located at the Istituto Motori CNR of Naples, are firstly described. A decompression and distribution system allows to feed the MGT with gaseous fuels characterized by different compositions. Moreover, a system of remote monitoring and control together with a data transfer system have been developed in order to set the operative parameters of the machine for the current test. The results of the tests performed under different operating conditions are then presented. Subsequently, the paper presents the numerical analysis of a model of the MGT combustor. The combustor model is validated against manufacturer performance data and experimental data with respect to steady state performance, i.e. average outlet temperature, emission levels, pressure drops.

Then, a syngas, composed by different ratios of hydrogen, carbon monoxide, methane, carbon dioxide and water, is simulated and the results analyzed.

### **INTRODUCTION**

In recent years, the interest in renewable energy sources has electricity demand, which is strongly influenced by the improvement of living standards, the decline in availability of fossil fuels and the concomitant need to reduce pollutant emissions. In this context, biomass plants represent a strategic resource useful to reduce greenhouse emissions such as carbon dioxide. Biomass exploitation allows the use of different technologies for power generation in small and medium scale plants.

Among renewable sources, biomass plays a key role because it can be considered as a programmable energy source. This feature is a definite advantage in distributed power generation, because of the unpredictability of renewable energy sources, like solar and wind power, that proved to be critical for voltage and frequency grid stability.

The term biomass denotes any organic substance derived directly or indirectly from photosynthesis, thus representing a large number of very heterogeneous raw materials (residues from crops, forestry residues, waste from wood processing industry, farm wastes, aquatic algae, organic fraction of municipal solid wastes).

The use of the energy content of biomass in closed combustion systems requires the conversion of biomass into more usable substances. Conversion processes can be divided into two main groups: biochemical processes and thermochemical processes. Among thermochemical processes, gasification and pyrolysis have a particular interest since they

provide the final product as the "synthesis gas" (syngas) that can be used directly as fuel in internal combustion power systems [1]. The fuel obtained is characterized by different compositions and properties, that depend on i) the type of biomass, ii) the conversion process, iii) the process parameters [2, 3, 4]. The systems used in energy production from biomass based on gasification processes commercially available consist of (i) an apparatus for biomass loading, (ii) a gasifier (typically downdraft), (iii) a complex apparatus for cleaning producer gas and (iv) a set of internal combustion engines. From an economic point of view, these systems have proven to be the least profitable among the established systems for energy production from biomass [2], especially because of the high operating costs (maintenance and disposal of ashes) and the low overall conversion efficiency.

In this context, the interest in the use of synthesis gas in micro gas turbines has considerably increased. Micro gas turbines allow to use syngas characterized by an higher level of contamination than that used in internal combustion engines [5], which implies: (i) the possibility of simplifying the apparatus for cleaning producer gas and hence a consequent reduction of investment and operational costs [6] and (ii) the possibility of using updraft gasifiers that allows to obtain a greater overall conversion efficiency also using gas with an higher concentration of tar [7] [8] [9].

The present work grows out of a collaboration among the Istituto Motori CNR of Naples, the Energy Systems Research Group of the Engineering Department of University of Ferrara and Turbec SpA, the manufacturer of the Micro Gas Turbine under consideration.

The aim of the overall project is to develop innovative technologies and processes in order to increase efficiency and reduce pollutant emissions in power generation systems based on micro gas turbines fed by biofuels. In particular, the activity developed by Istituto Motori and University of Ferrara has been focused on the use of gaseous biofuels for distributed power generation. This activity started by a realization of a test bench for the MGT Turbec T100, a Micro Gas Turbine with a nominal power equal to 100 kW<sub>el</sub>, and a parallel development of a model for numerical simulation of the MGT combustor.

The present paper presents a numerical study of Turbec T100 combustion chamber fed by natural gas and synthesis gas (syngas) obtained by biomass gasification. The performance of the combustor has been analyzed under different operating conditions such as fuel distribution between the two supply lines and the mass flow of air pumped by the compressor. The aim of the investigation is to identify the main features of combustion phenomena in case of syngas feeding with respect to natural gas feeding, for which the combustor has been designed.

The MGT has been installed in a test rig in the laboratory of CNR of Naples. The MGT has been instrumented for run under different operating conditions. A plant for decompression and distribution of fuel gas mixtures allows to feed the

combustor by fuels with different composition. Finally, a remote monitoring and data transfer system have been realized.

## NOMENCLATURE

CHP	Combined Heat and Power
LHV	Lower Heating Value
MGT	Micro Gas Turbine
TIT	Turbine Inlet Temperature
TOT	Turbine Outlet Temperature

## TEST-BENCH DESCRIPTION

The MGT Turbec T100 has been installed in a test rig in the laboratory of CNR of Naples. The micro gas turbine is an energy system for combined heat and power production, with a regenerative cycle, which generates 100 kW of electrical power with an overall CHP efficiency equal to 77 %.

Table 1 shows the main technical data stated by the manufacturer [10].

The MGT is a single-shaft micro gas turbine (Figure 1), with a two-pole permanent magnet mantled on the same shaft as the compressor/turbine and that rotates at the same speed. The high-speed generator produces high frequency electricity, which is converted to the main frequency and voltage in the power converter. The electrical system is entirely controlled and automatically operated by the Power Module Controller (PMC). The combustion chamber is a reverse flow tubular combustor with a regenerator for recovering part of the enthalpy of the exhaust gases. The geometry of the combustion chamber is shown in Figure 1, in which it is possible to notice the dilution holes located at the end of the liner and the annular conduit for air coming from the compressor. Moreover, for CHP applications there is a gas-water counter-current heat exchanger (the thermal energy from the exhaust gases is transferred to the hot-water system by the heat exchanger. The exhaust gases leave the heat exchanger through an exhaust pipe and the subsequent chimney).

### Design of a power plant for hydrogen-mixtures supply.

In order to allow a MGT supply with fuels characterized by a variable composition (with a certain percentage of hydrogen), a decompression and distribution plant for fuel gas mixtures has been realized.

The plant was designed to use gas mixtures consisting of methane, hydrogen, nitrogen, carbon dioxide, using tanks with a maximum pressure equal to 200 bar. The system is based on a pressure reduction system complete with ramps connecting to cylinders and/or bundles of cylinders where the gas pressure is reduced to 10 bar. An environmental monitoring system can detect leaks of flammable gases in the workplace. The middle relief has been designed for a rated capacity of fuel gas equal to 100 Nm<sup>3</sup>/h. This flow rate is more than double the nominal value, calibrated to run on natural gas (40 Nm<sup>3</sup>/h).

**Table 1.** Turbec T100 technical data.

Electric Power	100kW
Electric efficiency	30 %
Pressure in combustion chamber	4.5 bar
Turbine Inlet Temperature (TIT)	950 °C
Turbine Outlet Temperature (TOT)	620 °C-650 °C
Nominal speed	70000 rpm
NO <sub>x</sub> @ 15 % O <sub>2</sub>	< 15 ppm
CO @ 15 % O <sub>2</sub>	< 15 ppm
<b>CHP version</b>	
Thermal power (water @ 70-90 °C))	155 kW
Overall Efficiency* @ 70-90 °C	77 %
Thermal Efficiency	47 %

\*: represents the sum of electric and thermal efficiencies.

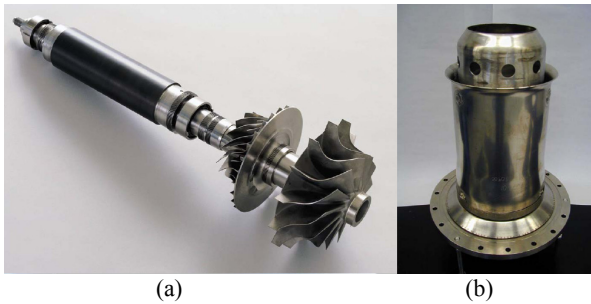


**Figure 1.** MGT components: (a) single-shaft micro gas turbine and (b) combustor chamber.

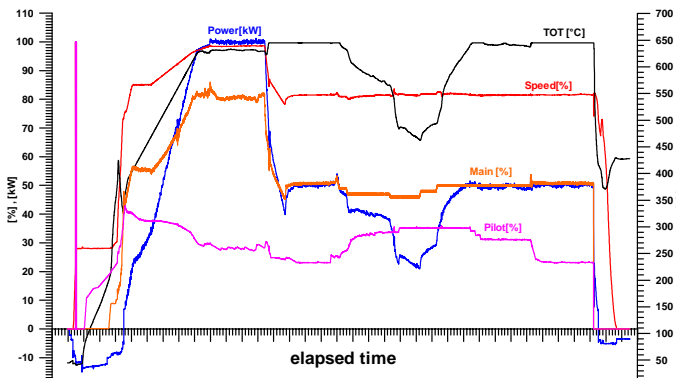


**Figure 2.** MGT operational parameters in “internal control”.

This design feature was made to allow the use of low calorific values fuels that requires higher values of mass flow rates in order to have constant power output from the microturbine. The gas is piped through stainless steel AISI 316L duct line until the point of use, located inside the test room (near the MGT fuel supply system).

**MGT control and remote monitoring system and data transfer system.** The MGT is managed through a remote control /monitoring system and then a data transfer system. The system for control and monitoring is located in the control room near the testing room and is constituted by a line for data transfer from the machine programmable logic controller (PLC) to the control room (location of calculation) and a system for

data acquisition. The system provides a remote control via Internet browser thanks to which it is possible to start/stop the MGT and to capture the main operation parameters, such as electric power and rotational speed and hence it is possible to know the MGT time-history. Moreover, it is possible to access to the remote system using an Ethernet connection.

The data transfer between the PLC and the MGT calculation station is obtained using a serial Modbus® communications protocol. Data transmission is achieved by means of an asynchronous serial converter (SENECA S107USB) that converts the RS485 signal to a PLC signal on the USB standard to be sent directly to the computer. A dedicated software (SENECA Z-NET3) [11] allows a direct interface to the register data of MGT, allowing to read all serial data.

The MGT operating parameters coming from the sensors are implemented in the machine room with a maximum sampling rate equal to 1 Hz.

The acquisition system is designed in a modular form to enable the implementation of additional signals from sensors and additional tools (e.g., temperature and pressure in the combustion chamber, flue gas analysis instruments, fuel flow measurement, etc.). In particular, it was designed for the simultaneous acquisition of up to 64 analog/digital channels.

The management software of commercial machines is able to autonomously manage the proper functioning of the MGT, with the user enabled to control only the required electric power. All the other operating parameters of the machine are "optimized" according to a functioning map provided by the manufacturer (internal control functioning).

The experimental tests require a system open enough to vary some parameters, such as the air/fuel ratio, the fuel distribution between the two supply lines, the type of fuel, etc.. For this reason, some modifications have been made on the software in order to exercise the machine in user-defined working points that lie out of the standard map thanks to the variation of MGT operating parameters (though maintaining the intrinsic safety of the trading system).

Implementing the so-called external control, it is possible to define the set point referred to the rotational speed (and thus the mass flow of combustion air), the opening level of the main valve (primary burner fuel mass flow) and the pilot valve (pilot burner fuel mass flow). The set points can be set via analog inputs controlled by a PC placed in the control room. The variable control is done via analog signals in current (4-20 mA).

Figure 2 shows the trends of the main operational parameters when the MGT works in internal control. The machine parameters are fully managed in accordance with the original software based on the internal operation map. The test was carried out at full load (100 kW<sub>el</sub>) and at partial load (50 kW<sub>el</sub>).

**Measurement of fuel mass flow.** In order to determine the fuel mass fed to the combustion chamber, two mass flow meters were installed on the fuel lines for the main and the pilot burners, respectively. Two digital thermal mass flow meters

(Bronkhorst High-Tech, EL-FLOW Select) were used. This class of sensors permitted to measure the mass flow rates with an accuracy of  $\pm 0.8\%$  R plus  $\pm 0.2\%$  FS. The data acquisition from the instruments is made via analog signals in current (4 – 20 mA), implemented in the MGT data transfer system.

The experimental tests were carried out in “internal control” mode. In this configuration it is possible to just set the electrical power load, with the MGT that tracks the working points of the standard operation map.

During the experimental run, the operational parameters of the microturbine and the fuel mass flows in the primary and secondary fuel lines have been acquired. Furthermore, through the PC based data transfer system, it has been done the monitoring of the emissions in the exhaust gases.

**MGT exhaust emissions measurement.** The portable flue gas analyzer (TESTO 350 S) has been used for the monitoring of the exhaust emissions. The measurement system utilizes electrochemical cells, and an IR-sensor for the detection of gaseous pollutants in the exhaust of the MGT.

The flue gas analyzer is equipped with electrochemical sensors (cells) for the detection of  $O_2$ , NO,  $NO_2$ , CO,  $SO_2$  and an infrared sensor for the detection of  $CO_2$ . By a serial port connection the system is connected to a PC; a software installed manages all the functions of the analysis system and records data with a maximum sampling rate of 1 Hz. The measured pollutants concentrations were corrected to be conventionally reduced to 15 %  $O_2$  content. Table 2 presents the measurement range of the cells.

## CFD ANALYSIS

**Combustion chamber geometry.** The Figure 3 shows the combustion chamber of MGT Turbec T100, in which the main components are highlighted using different colors. The *inner flame tube* (the inner wall of the combustion chamber necessary to contain the flame) is highlighted in red, while the *outer flame tube* (that encloses the volume obtained for air flow) is colored in blue. In the final area of the inner flame tube there are nine dilution holes in order to reduce the temperature of flue gas. The fuel is divided in two different lines: the pilot line (diffusive) and the main line (premixed). The nozzle of the pilot line is coaxial with the combustion chamber and it directly introduces the fuel into the primary zone, while the main line is not coaxial with the combustion chamber and it introduces the fuel into a chamber connected with the secondary zone.

The air pumped by the compressor enters in the combustion chamber in countercurrent with respect to combustion gases, passing through the space between outer and inner flame tube. Part of the incoming air enters to the dilution holes, while the remaining mass flow arrives to the primary and the secondary swirlers. The primary and secondary swirlers provide the air to the pilot (primary zone) and main (secondary zone) burners, respectively. In the primary swirler the seat for the spark needed to start-up of the microgasturbine has been obtained.

**Computational domain.** The geometry of the combustion chamber, shown in Figure 3, has been modeled using SolidWorks 2010. The geometry of the combustor of Turbec T100 is axisymmetric, but it presents different periodicities when the number of channels of primary and secondary swirlers and the dilution holes are considered. Therefore, it was unfeasible to reduce the angular computational domain, and the whole fluid domain has been considered in the calculations.

**Grid.** The discretization of fluid domain was performed using the commercial code ANSYS ICEM CFD 12.0 that allows the generation of volumetric tetrahedral and hexahedral unstructured grids. The mesh used for the CFD analyses is a hybrid grid (tetrahedral and hexahedral grid elements). In particular, it consists of:

- tetrahedral elements in the zone in correspondence of the base of the combustor where the shape of the geometry is characterized by a major complexity. This zone is essentially constituted by the conduits for fuel delivery, the swirlers, the stator vanes and the primary combustion zone;

Table 2. Test measurement species and ranges.

Species	Meas. range	Accuracy
$O_2$	0÷25 Vol. %	$\pm 0.8\%$ fs
CO	0÷500 ppm	$\pm 2$ ppm
NO	0÷300 ppm	$\pm 2$ ppm
$NO_2$	0÷500 ppm	$\pm 5$ ppm
$CO_2$	0÷50 Vol. %	$\pm 0.3$ Vol %

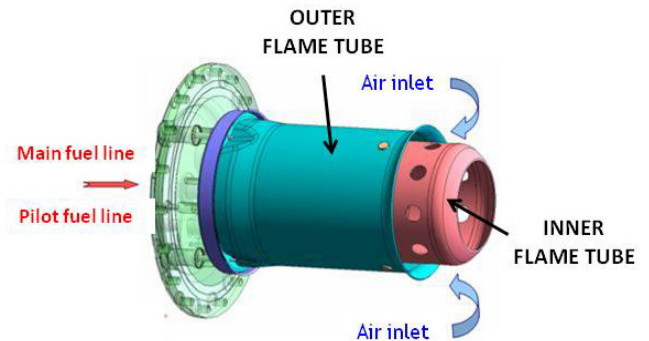


Figure 3. Combustion chamber of Turbec T100.

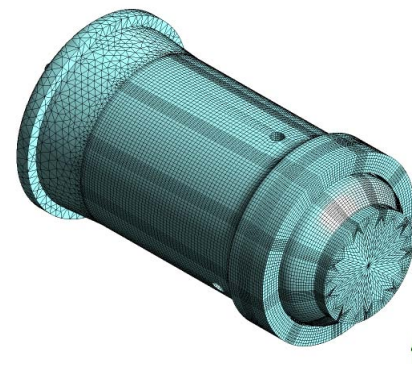


Figure 4. Hybrid grid generated using ICEM CFD 12.0.

- hexahedral elements corresponding to the areas characterized by large and quite regular fluid domains, as the secondary combustion zone and the zone from air inlet.

The two grids have been separately generated and, then, merged to form one hexahedral-tetrahedral hybrid mesh with an overall number of elements approximately equal to 1'500'000 (Figure 4). In order to perform a grid sensitivity analysis, the numerical results obtained by using the hybrid grid have been compared with those obtained using a tetrahedral grid with about one million elements and a tetrahedral grid with about 2'000'000 elements. The tetrahedral-hexahedral hybrid grid allows to achieve a better numerical convergence than the fully tetrahedral grids: the residual values on the balance equations are up to two orders of magnitude lower and the graphs show a more stable trend of the convergence. The hybrid grid used for calculations is robust with respect to the overall performances of the combustor in terms of pressure distribution within the combustor, thermal power, and turbine inlet temperature. From a qualitative point of view, no significant change in velocity profiles and distributions of temperature, pressure and chemical species concentration has been noticed.

For these reasons, the hybrid grid has been used in the numerical analyses presented below.

**Numerical models.** The numerical models used in CFD calculations have been defined through a sensitivity analysis carried out in order to define the models able to better predict the real behavior of the combustor. The following models have been implemented in all the numerical calculations presented in the paper:

- **turbulence model:** BSL-RSM, i.e. Reynolds Stress Model (RSM) based upon the transport equation of  $\omega$  (BSL). The RSM models solve 6 transport equations (one for each of the six components of the Reynolds stress tensor) and the transport equation for a characteristic parameter of turbulent dissipation. In the case of BSL model, the additional equation is based on the turbulent frequency  $\omega$  (defined by the ratio of turbulent kinetic energy dissipation  $\varepsilon$  on turbulent kinetic energy  $k$ ). For the boundary-layer analysis, the BSL-RSM model uses an analytical expression for  $\omega$  in the viscous sublayer [12][13];

- **combustion model:** combined Eddy Dissipation Model/Finite Rate Chemistry (EDM/FRC). This model (which has proved to be the most reliable since there is the simultaneous presence of diffusive and premixed combustion) is based on the comparison of the characteristic time of the two following models: (i) FRC model, in which the chemical reaction rate is determined through the Arrhenius law and (ii) EDM model that is based on the assumption that the rate of reaction depends on the time needed to mix the reagents at molecular level. The combined model EDM/FRC takes as the actual reaction rate the minimum value of the two models [10, 12];

- **reaction mechanism:** the 2-step Westbrook and Dryer for methane oxidation, 1-step Westbrook and Dryer for hydrogen oxidation and the Zeldovich mechanism for NO formation [12].

**Boundary conditions.** The boundary conditions applied to CFD analyses are shown in Figure 5. The overall fuel mass flow is divided in the two supply lines (main and pilot) and hence for each inlet surface the respective value of mass flow has been set. The value of the fuel inlet temperature has been set to room temperature (20 °C). Also on the air inlet surface the values of mass flow, composition and temperature have been set. The composition of combustion air is supposed to consist only of oxygen and nitrogen, with mass fractions equal to 0.23 and 0.77, respectively. The temperature value has been established in relation to the experimental data provided by the manufacturer. On the outlet surface a value of the static pressure equal to the compression ratio has been imposed. On the remaining surfaces of fluid domain, a wall condition has been set: for the inner and outer walls a value of temperature equal to 1000 K and 600 K has been imposed, respectively, while on the other surfaces an adiabatic condition has been set.

**CFD results: natural gas feeding.** In order to evaluate the fluid dynamic behavior of the combustion chamber under consideration, preliminary CFD analyses have been carried out using the numerical models yet described in the previous section. Numerical simulations are referred to the full load operation condition (100 kW<sub>el</sub>) in case of methane feeding. At first, a fluid dynamic analysis has been presented in terms of 2D stream lines plotted on a longitudinal plane. As it can be seen in Figure 6, the stream lines present the typical morphology of this particular type of combustors: the corner vortexes located in the corner regions and two counter-rotating vortexes located in correspondence of the secondary combustion zone (between the dilution holes and the outlet surface).

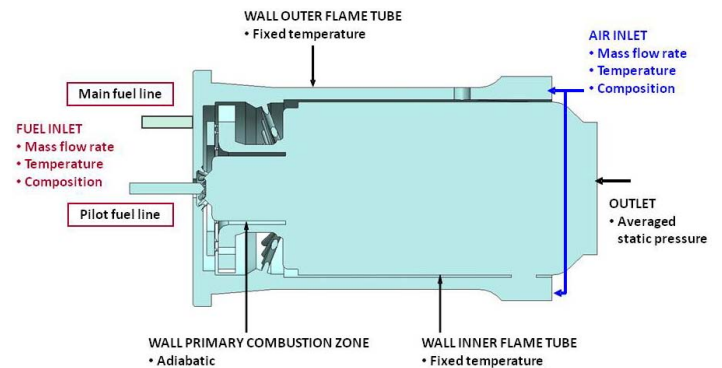


Figure 5. Boundary conditions used in numerical calculations.

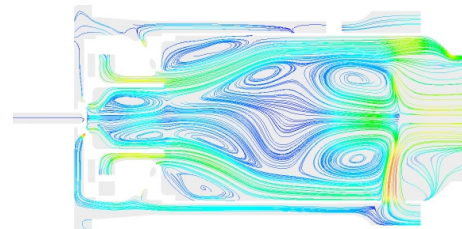


Figure 6. Stream lines for the standard fuel distribution (15 % at pilot line and 80 % at main line).

In the numerical simulation, a reference fuel distribution between the two supply lines has been considered (15 % to pilot line and 85 % to main line). In order to understand the influence of a different distribution of the fuel on the combustor behavior, four additional fuel distributions have been considered in the numerical analysis: (a) 20 % at pilot line and 80 % at main line, (b) 30 % at pilot line and 70 % at main line, (c) 65 % at pilot line and 35 % at main line and (d) 85 % at pilot line and 15 % at main line. The fuel distributions (c) and (d) can be considered representative only for the MGT start-up operating phase.

As can be noticed in Figure 7, the fluid dynamic behavior of the combustor is not significantly affected by the fuel distribution. In fact, the morphology and the position of the vortices are not modified in a significant way. On the contrary, the temperature distribution is strongly influenced by fuel distribution in terms of flame morphology: in particular, with the increasing of the percentage of fuel in the pilot line it can be noticed a reduction of the temperature in correspondence of the primary combustion zone and a displacement of the flame towards the combustor axial position. Moreover, outside the primary combustion zone, the morphology of the flame does not change: in all cases there is a bifurcation of the flame due to the presence of two vortices (still visible in Figure 8) in the central area of the combustion chamber, symmetrical to the combustor axis. The variation in the morphology of the flame is also confirmed by the different CH<sub>4</sub> mass fraction distributions inside the fluid domain. In fact, in case of a small percentage of fuel to the pilot line, there is a consumption of CH<sub>4</sub> yet at the exit of the pilot line itself, while the increasing of fuel mass flow in pilot line determines a fuel consumption in correspondence of the exit zone of fuel from the main line and the air from the secondary swirler. Moreover, also a variation in the local CO and CO<sub>2</sub> distribution has been noticed: the variation in CO distribution is observable only locally being not identifiable in the global examination. On the contrary, the NO<sub>x</sub> concentration at the combustor outlet surface is influenced by the different fuel distribution considered.

Table 3 presents a comparison between the values of turbine inlet temperatures (TIT) obtained from the CFD analyses performed and the experimental value of a preliminary test. It can be noticed that the overall energy balance does not present significant differences between the studied cases. Hence, it is possible to observe that the thermal power developed within the combustion chamber, and so the temperature of gases leaving the combustion chamber, are not influenced by the fuel distribution between the two supply lines.

**Table 3.** Values of TIT reported in K (P: pilot line and M: main line).

<i>Experimental</i>	<i>Numerical</i>	
1223	P15 % - M85%	1202
	P20 % - M80%	1199
	P30 % - M60%	1200
	P65 % - M35%	1202
	P85 % - M15%	1203

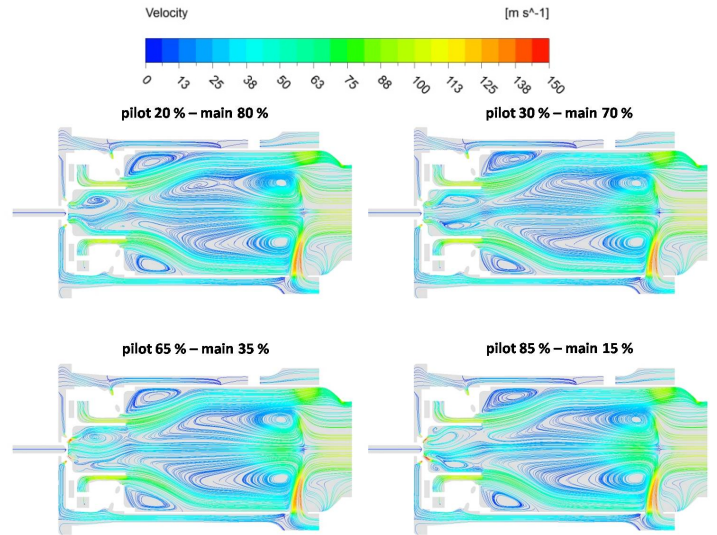


**Figure 7.** Streamlines in a longitudinal plane.

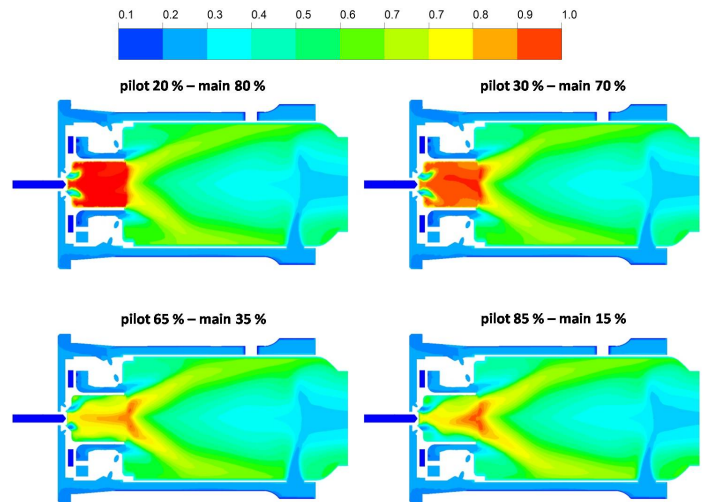


**Figure 8.** Temperature distribution in a longitudinal plane.

**CFD results: LHV fuel feeding.** Finally, a preliminary analysis of the performance of the combustor in case of feeding with a fuel obtained through biomass gasification process has been performed without changing the geometry of the combustor (originally designed for natural gas combustion). In particular, a syngas produced by a pyrolyzer installed at the University of Perugia and obtained from forestry wastes was considered [15]. The composition of the syngas is: 7% H<sub>2</sub>, 29% CO, 21% CH<sub>4</sub>, 38% CO<sub>2</sub>, 5% H<sub>2</sub>O (volume percentage) and the calorific value (dry basis) is equal to 9400 kJ/kg [8].

For the numerical simulations, the same boundary conditions of the natural gas supply case have been set, except for the fuel mass flow and its composition. In order to perform a comparable simulation, the syngas mass flow has been determined so that the input thermal power would be the same of the case of methane supply.

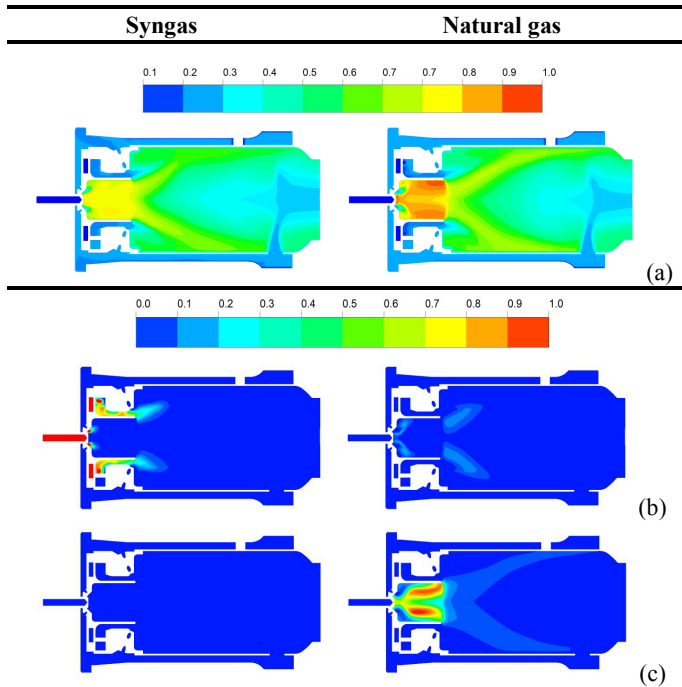


**Figure 9.** Non-dimensional distribution in a longitudinal plane of: (a) temperature, (b) CO molar fraction and (c) NO molar fraction.

For the calculations a standard fuel distribution has been imposed: 15 % to the pilot line and 85 % to the main line. As can be seen from the comparison between the results referred to methane and syngas feeding (Figure 9), the use of a synthesis gas allows to obtain lower temperature values within the primary combustion zone, with a consequent reduction in  $\text{NO}_x$  formation (14.9 ppm@15% $\text{O}_2$  in case of natural gas combustion and 0.5 ppm@15% $\text{O}_2$  in case of syngas combustion). These results are in accordance with both phenomena related to the combustion process of LHV fuels from biomass described in literature [16][17][18] and results provided by other studies which consider MGTs in the range (1-100) kW<sub>el</sub> fed by LHV fuels [19][20][9].

## COMPARISON OF CFD RESULTS WITH PRELIMINARY EXPERIMENTAL RESULTS

In the present section, some preliminary experimental tests performed on the MGT Turbec T100 are presented. A comparison between the experimental results and the results of CFD numerical simulations are reported. The comparison is not a validation of the CFD results (which need a more thorough insight and a more comprehensive test campaign) but an assessment of the methodology developed.

**Experimental test.** The experimental test has been carried out in "internal control", setting just electrical power reference. The experimental parameters of the test under consideration are reported in Table 4. The table shows that the maximum electric power obtained was equal to 90.1 kW<sub>el</sub> (lower than the MGT nominal electric power equal to 100 kW<sub>el</sub>). This was due to the high air inlet temperature (28.3 °C) during this preliminary test.

**Table 4.** Experimental parameters.

Electric Power [kW <sub>el</sub> ]	80.3	90.1
Fuel volume flow rate [Nm <sup>3</sup> /h]	27.4	30.7
Turbine Outlet Temperature [°C]	641.9	642.2
T air inlet [°C]	28.5	28.3
Rotational speed [rpm]	66780	69300
<i>Emissions</i>		
NO <sub>x</sub> [ppm@15%O <sub>2</sub> ]	11	9
CO [ppm@15%O <sub>2</sub> ]	2	2

Then, a part load operating point was gathered by imposing the set point to  $P_{el} = 80$  kW<sub>el</sub>. At this time, the available experimental results concern the emission levels (NO<sub>x</sub> and CO) and the Turbine Outlet Temperature (TOT). The TIT is not measured (as usually done in practice) but is inferred through the TOT by means of a Cycle Deck calculation. The Cycle Deck calculation is based on thermodynamic balances and on the compressor and turbine performance maps, which are proprietary of the manufacturer. From a calculation performed at 90 kW<sub>el</sub>, the estimated TIT resulted equal to 1193 K, while at 80 kW<sub>el</sub> the TIT estimated value was 1180 K.

**Numerical results.** Different CFD analyses have been implemented using the experimental data reported in Table 4. The methodology and the model used are the same used in the previous paragraph as in the case on natural gas feeding.

*Baseline simulation.* In the first simulation, the fuel mass flow rate corresponding to the volume flow rate as in Table 4 for the working load at 90.1 kW<sub>el</sub> was used as fuel inlet boundary condition. The air volume flow rate at the combustion chamber inlet was set, as a first tentative, to the design one ( $m = 0.7658$  kg/s) since no experimental data were available.

In Figure 10 the temperature distribution in a longitudinal and a transversal plane is presented in the case of the working load at 90.1 kW<sub>el</sub>. The transversal plane is in correspondence of the section A indicated in the figure on the left and it corresponds of the middle section of the main line supply ducts. It can be noticed that the temperature distribution reported in Figure 10 is similar to the one reported in Figure 9 (referred to the nominal power operating condition). The temperature distribution is represented in a non-dimensional scale between the minimum and the maximum value of the local temperature on the two considered planes.

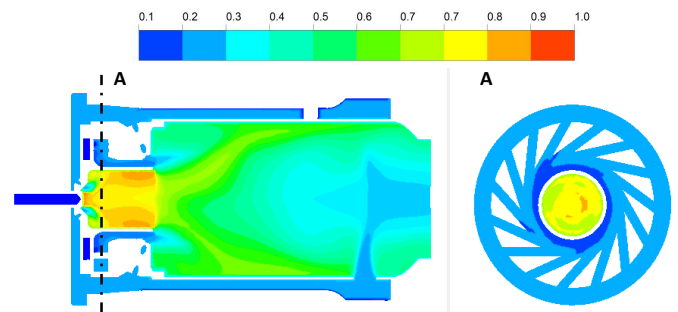


**Figure 10.** Non-dimensional temperature distribution in a longitudinal and a transversal plane (*baseline case*).

The temperature levels are lower than the corresponding one at full load due to both a reduction of the thermal power input and the more dilution of the mixture.

Figure 11 shows the 3D stream lines inside the combustor. The images on the left show the stream line referred to air arriving from the primary swirler and fuel arriving from the pilot line, while the images on the right show air arriving from the secondary swirler and fuel arriving from the main line. In all pictures air stream lines are colored in light blue and fuel ones are colored with the CO<sub>2</sub> molar fraction (in order to understand in which areas combustion occurs). The images show the local mixing between air and fuel and the combustor zones in which combustion takes place.

**Sensitivity analysis on inlet boundary conditions.** Five numerical simulations have been performed considering different fuel distributions and combustion chamber inlet air mass flow values. All results are reported in Table 5. This was done in order to perform a sensitivity analysis on the boundary conditions imposed to assess the effectiveness of the simulations in reproducing the effect of the variations of the actual operating conditions. The first analysis refers to the baseline case and, thus, the numerical calculation has been performed considering the standard value of the air mass flow (0.7658 kg/s). A standard fuel distribution between the two fuel supply lines (15 % to pilot line and 85 % to main line) has been also implemented. It can be noticed that the numerical value of TIT underestimates the estimated TIT value of about 30 K.

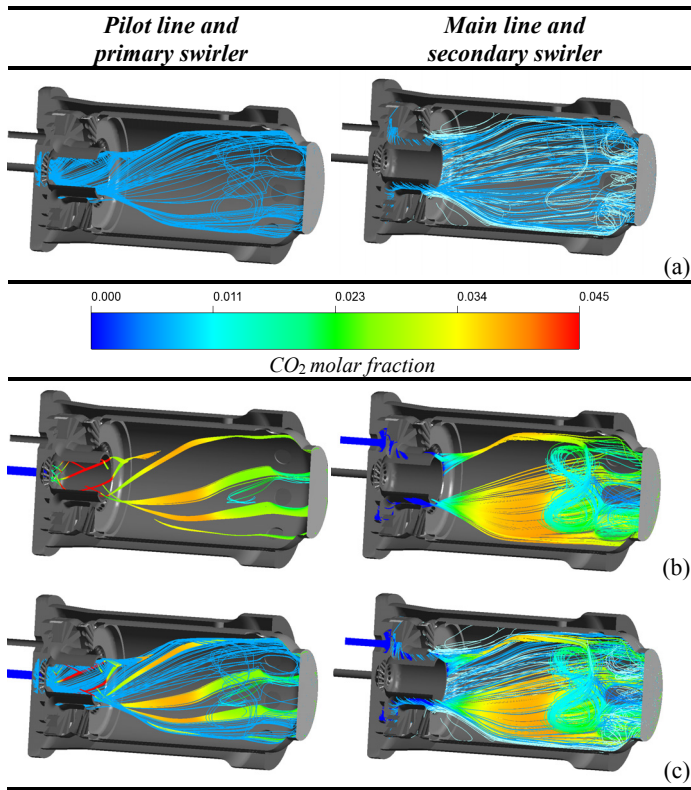


**Figure 11.** Streamlines: (a) air stream lines, (b) fuel stream lines and (c) air and fuel stream lines.

Since a different fuel distribution has been measured (13 % to pilot line and 87 % to main line), a second CFD analysis has been carried out (case *a*) using the new value of fuel mass flow in the two supply lines. From a comparison between cases *baseline* and *a*, it can be noticed that a reduction of the fuel mass flow to the pilot line equal to 13 % strongly reduces the NO emissions, while the TIT is still underestimated.

For this reason, a lower value of the air mass flow equal to 0.70 kg/s has been considered (case *b*). This value was chosen accordingly to Cycle Deck calculations and to personal communications with the manufacturer. This calculation and the following ones have the meaning of a sensitivity analysis on the air inlet boundary conditions. For this numerical analysis, a standard fuel distribution has been defined (15 % pilot and 85 % main). Table 5 shows that the air mass flow for case *b* allow to obtain a better prediction of experimental results. In fact, both the values of pollutant emissions are in good accordance with the experimental ones, and the calculated TIT is closer to the estimated one.

In case *c* the measured fuel flow rates were set (13 % pilot, 87 % main). The comparison between cases *b* and *c* confirms that a reduction of the fuel mass flow to pilot line allows decreasing of NO emissions in correspondence of the combustor outlet surface, without varying the value of the TIT (only influenced by the total thermal power input and so by the overall fuel mass flow).

Finally, the influence of a further reduction in the air mass flow ( $m = 0.68$  kg/s) has been investigated in case *d*. It is possible to noticed that with decreasing in air mass flow rate equal to 11 % the values of TIT reaches 1240 K and NO emission are higher than 50 ppm@15%O<sub>2</sub>.

For all the considered cases the numerical values of CO emissions present a good agreement with the numerical value, even if in general the 2-steps combustion reaction mechanism underestimates experimental values.

Figure 12 shows the temperature distributions for all the considered cases. It can be noticed that a variation of fuel distribution from a standard value (*baseline* case: 15 % to pilot line and 85 % to main line) to the distribution of case *a*: 13 % to pilot line and 87 % to main line does not determine a significant variation in temperature field distribution plotted on the transversal plane, but only a reduction in terms of temperature values in the primary zone (diffusive combustion zone). As a consequence, the NO emission values decrease in the cases in which the temperature values in the primary zone are higher (according to [16]). In case of mass flow air  $m = 0.70$  kg/s (case *b* and *c*) the temperature distributions do not vary with respect of cases with the standard value of mass flow air (*baseline* and *a*) and also between each other.

On the contrary, the decreasing in the air mass flow determines a temperature values increasing in the primary combustion zone (cases *b* and *c*).

For the case *d* in can be noticed that a reduction of the mass flow air value produces the increase in temperature value especially in the primary combustion zone.

**Table 5.** Numerical sensitivity analysis of air mass flow and fuel distribution between the two supply lines (load@90.1 kW<sub>el</sub>).

	TIT [K]	CO@15%O <sub>2</sub> [ppm]	NO@15%O <sub>2</sub> [ppm]
<i>baseline</i>	1163	1	4
<i>a</i>	1162	1	1
Numerical <i>b</i>	1187	1	13
<i>c</i>	1187	1	7
<i>d</i>	1240	1	55
Experimental*	1193	2	9

(*baseline*) Standard fuel distribution: 15 % to pilot and 85 % to main. Standard air mass flow: 0.7658 kg/s; (*a*) Fuel distribution: 13 % to pilot and 87 % to main. Standard air mass flow: 0.7658 kg/s; (*b*) Standard fuel distribution: 15 % to pilot and 85 % to main. Air mass flow: 0.70 kg/s; (*c*) Fuel distribution: 13 % to pilot and 87 % to main. Air mass flow: 0.70 kg/s; (*d*) Standard fuel distribution: 15 % to pilot and 85 % to main. Air mass flow: 0.68 kg/s; \*: chosen accordingly to Cycle Deck calculations.

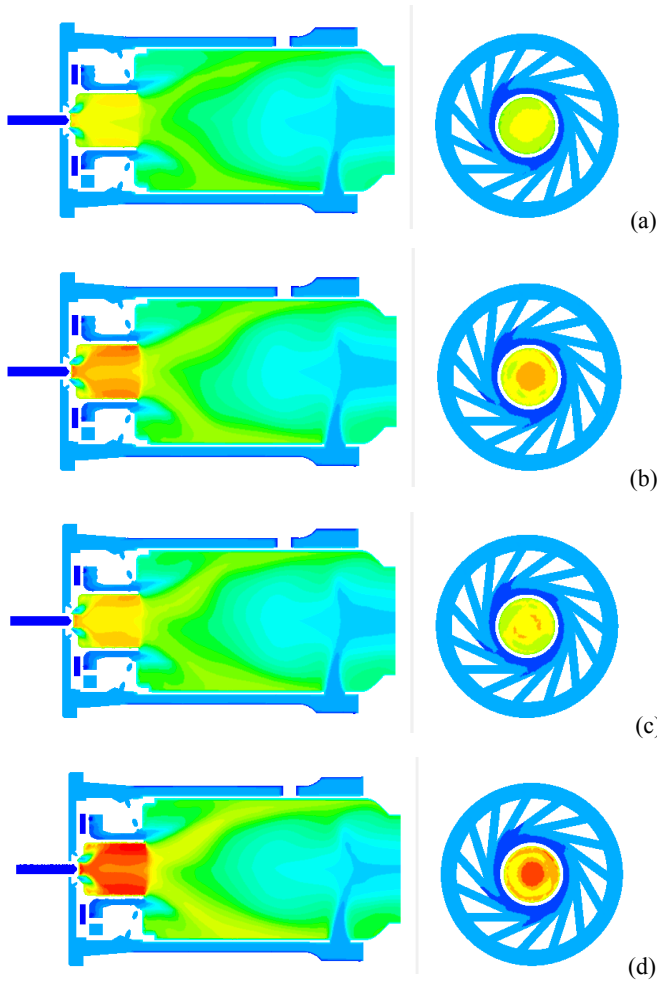


**Figure 12.** Temperature distribution in a longitudinal and a transversal plane (cases *a*, *b*, *c* and *d*).

**Table 6.** Numerical and experimental data (load@80.3 kW<sub>el</sub>).

	TIT [K]	CO [ppm@15%O <sub>2</sub> ]	NO [ppm@15%O <sub>2</sub> ]
Numerical**	1178	1	10
Experimental*	1180	2	11

\*\* Standard fuel distribution: 15 % to pilot and 85 % to main. Air mass flow: 0.640 kg/s; \*: chosen accordingly to Cycle Deck calculations.

**Part load simulation.** Finally, the simulation referred to the working point @ 80.3 kW<sub>el</sub> has been performed. The value of inlet air mass flow (0.640 kg/s) was chosen accordingly to Cycle Deck calculations.

The comparison between numerical and experimental results is presented in Table 6. It can be noticed that the data are in good agreement, in particular in terms of NO concentration and TIT. In fact, the numerical value of CO concentration underestimates the experimental one (due to the 2-step reaction mechanism).

In Table 7 a comparison between experimental data and numerical results in terms of physical parameters at the combustor outlet surface (TIT, CO and NO concentrations) is summarized for the two working points described before. As a conclusion, it can be stated that, even if at a preliminary stage evaluation, the numerical calculations and the simulation methodology is able to reproduce the combustor overall behavior.

## CONCLUSIONS

The paper describes the experimental apparatus designed for the experimental test conducted on the micro gas turbine Turbec T100. The micro turbine has been installed in a test rig in the laboratory of CNR of Naples and it has been instrumented for run under different operating conditions. A plant for decompression and distribution of fuel gas mixtures allows to feed the combustor by fuels with different composition. Finally, a remote monitoring and data transfer system has been realized. A numerical study performed on the Turbec T100 combustor chamber fed by natural gas and synthesis gas obtained by gasification of biomass. The performances of the combustor have been analyzed under different operating conditions such as the distribution of fuel between the two supply lines and the mass flow of air pumped by the compressor.

**Table 7.** Numerical and experimental data for the operating points.

Load	Parameter	Numerical results	Experimental data
90.1 kW <sub>el</sub>	TIT [K]	1187	1193
	CO [ppm@15%O <sub>2</sub> ]	1	2
	NO <sub>x</sub> [ppm@15%O <sub>2</sub> ]	7	9
80.3 kW <sub>el</sub>	TIT [K]	1178	1180
	CO [ppm@15%O <sub>2</sub> ]	1	2
	NO <sub>x</sub> [ppm@15%O <sub>2</sub> ]	10	11

The preliminary CFD analyses underline the following results: (i) the fluid dynamic behavior of the combustor is not significantly affected by the fuel distribution between the two supply lines; (ii) the temperature distribution is strongly influenced by fuel distribution in terms of flame morphology; in particular, with the increasing of the percentage of fuel in the pilot line it can be noticed a reduction of the temperature in correspondence of the primary combustion zone and a displacement of the flame towards the combustor axial position; (iii) the use of a synthesis gas allows to obtain lower temperature values within the primary combustion zone, with a consequent reduction in NO<sub>x</sub> formation.

Some numerical computations have been compared with the experimental results performed on Turbec T100 MGT in correspondence of two operating points: 90.1 kW<sub>el</sub> and 80.3 kW<sub>el</sub>. The results analysis has been underlined the capability of numerical models in solving combustion phenomena using simple combustion reaction mechanisms.

However, further experimental tests will be carried out in order to acquire more experimental data useful to reach a better comprehension of the combustor behavior under different operation conditions and using different synthesis gas composition mixture. Moreover, the experimental data deriving by a more detailed test campaign will be used for a specific setup in boundary conditions of the additional CFD analyses.

## ACKNOWLEDGMENTS

The research was partially supported by the Italian Ministry of Economic Development within the framework of the Program Agreement MiSE-CNR "Ricerca di Sistema Elettrico".

## REFERENCES

- [1] L. Casarsa, D. Micheli, V. Pediroda, R. Radu, 2009, Investigations of Pyrolysis Syngas Swirl Flames in a Combustor Model, *ASME Paper GT2009-59610*.
- [2] R. Bettocchi, et al., 2010, Assessment of Energy Chains for Distributed Generation: Agricultural and Thermoeconomic Analyses within Emilia-Romagna Region, *Proc. of 23rd International Conference on Efficiency, Cost, Optimization, Simulation and Environmental Impact of Energy Systems*, Lousanne, CH.
- [3] F. Fantozzi, B. D'Alessandro, U. Desideri, 2007, An IPRP (Integrated Pyrolysis Regenerated Plant) Microscale Demonstrative Unit in Central Italy, *ASME Paper GT-2007-28000*.
- [4] S. Colantoni, S. Della Gatta, R. De Prosperis, A. Russo, F. Fantozzi, U. Desideri, 2010, Gas Turbines Fired with Biomass Pyrolysis Syngas: Analysis of the Overheating of Hot Gas Path Components, *ASME J. of Eng. for Gas Turbines and Power*.
- [5] P. Hasler, T. Nussbaumer, 1999, Gas Cleaning for IC Engine Applications from Fixed Bed Biomass Gasification, *Biomass and Bioenergy*, 16, pp. 385-395.
- [6] A. Cai, A.P. Carlucci, G. Colangelo, M. G. De Giorgi, A. de Luca, D. Laforgia, G. Minosi, A. Nuzzo, A. Scarpello, G. Starace, 2009, Analisi e Studi Relativi all'Ottimizzazione di un Impianto di Gassificazione e Cogenerazione a Biomasse Lignocellulosiche, *64° Congresso Nazionale ATI*.
- [7] S. Gillette, 2008, Comparison of Microturbines and Reciprocating Engine Generator Sets, *ASME Paper GT2008-51365*.
- [8] F. Fantozzi, P. Laranci, M. Bianchi, A. De Pascale, M. Pinelli, M. Cadorin, 2009, CFD Simulation of a Microturbine Annular Combustion Chamber Fuelled with Methane and Biomass Pyrolysis Syngas - Preliminary Study, *ASME Paper GT2009-60030*.
- [9] F. Fantozzi, P. Laranci, B. D'Alessandro, 2009, CFD Analysis of Combustion of Natural Gas and Syngas from Biomass Pyrolysis in the Combustion Chamber of a Micro Gas Turbine, *Proc. 8th Latin-American Congress on Electricity Generation and Transmission - CLAGTEE*.
- [10] www.turbec.com.
- [11] www.seneca.it.
- [12] ANSYS CFX, 2009, User Manual, Release 12.0.
- [13] W.P. Jones, and Launder, B.E., 1972, The Prediction of Laminarization with a Two-Equation Model of Turbulence, *Int. J. Heat and Mass Transfer*, vol. 15, pp. 301-314.
- [14] B. F. Magnussen and B. H. Hjertager, 1976, On mathematical models of turbulent combustion with special emphasis on soot formation and combustion, *16th Symp. (Int'l.) on Combustion*, The Combustion Institute.
- [15] R. Bettocchi, G. Bidini, M. Cadorin, A. De Pascale, P. Laranci, A. Peretto, A. Vaccari, 2009, Analisi CFD di una Camera di Combustione per Microturbina Alimentata con Gas Naturale e con Syngas da Biomasse, *64° Congresso Nazionale ATI*.
- [16] A.H. Lefebvre, 1999, *Gas Turbine Combustion*, Taylor&Francis.
- [17] S.R. Turns, 2000, *An Introduction to Combustion*, MCGraw-Hill.
- [18] P.D.J. Hoppesteyn, 1999, Application of Low Calorific Value Gaseous Fuels in Gas Turbine Combustors, Delft University Press.
- [19] M. Prussi, G. Riccio, D. Chiaramonti, F. Martinelli, 2008, Evaluation of a Micro Gas Turbine Fed by Blends of Biomass Producer Gas and Natural Gas, *ASME Paper GT2008-50236*.
- [20] C.H. Yang, C.C. Lee, J.H. Hsiao, C.H. Chen, 2009, Numerical analyses and experiment investigations of an annular micro gas turbine power system using fuels with low heating values, *Science in China Press*.